THE JOURNAL OF PHYSICAL CHEMISTRY Letters

Letter

pubs.acs.org/JPCL

Exploration of Structures of Two-Dimensional Boron−Silicon Compounds with sp^2 Silicon

Jun Dai,[†] Yu Zhao,[†] Xiaojun Wu,*[,‡] Jinlong Yang,[§] and Xiao Cheng Zeng*[,†,§]

[†]Department of Chemistry and Nebraska Center for Materials and Nanoscience, University of Nebraska-Lincoln, Lincoln, Nebraska 68588, United States

[‡]CAS Key Lab of Materials for Energy Conversion, Department of Materials Science and Engineering and Hefei National Lab for Physical Science at Microscale, University of Science and Technology of China, Hefei, Anhui 230026, China

[§]Department of Chemical Physics and Hefei National Lab for Physical Science at Microscale, University of Science and Technology of China, Hefei, Anhui 230026, China

Supporting Information

ABSTRACT: The most stable structures of two-dimensional (2D) boron−silicon (B−Si) compounds containing planar sp^2-bonding silicon (sp^2-Si) are explored using the first-principles calculation-based particle-swarm optimization method. Among 10 B−Si compounds considered, we find that for BSi_4, BSi_3, BSi, B_2Si, B_3Si, B_5Si, and B_6Si, each Si atom is bonded with three B or Si atoms within the same plane, representing a preference of planar sp^2-Si structure in B−Si compounds. For BSi_2 and B_4Si, the predicted lowest-energy structures entail a small out-of-plane buckling. Furthermore, a planar-tetracoordinated Si (ptSi) atom bonded with four B atoms within the same plane is observed in the lowest-energy structure of B_7Si compound. Dynamical stabilities of the predicted 10 2D B−Si compounds are confirmed via phonon-spectrum calculation. The lowest-energy 2D B−Si compounds are all metals, regardless of the B−Si stoichiometry considered in this study.

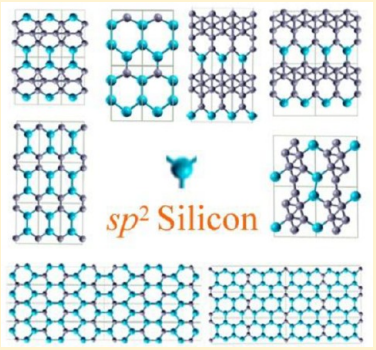

SECTION: Molecular Structure, Quantum Chemistry, and General Theory

Since the first isolation of two-dimensional (2D) graphene in 2004,[1−4] an era of exploring novel 2D nanomaterials has arisen. Although graphene is currently at the center stage of 2D materials research owing to its fascinating properties, such as massless Dirac Fermion and quantum Hall effect, research efforts toward other 2D materials in general and monolayer materials with single-atom-thickness in particular have increased considerably. For example, free-standing 2D boron-nitride (BN) monolayers have been successfully fabricated through a layer-by-layer sputtering process.[5] Monolayer MoS_2 sheets have also been isolated using micromechanical cleavage technique.[6] Coleman et al. reported a liquid exfoliation technique that can efficiently produce monolayer sheets of various of inorganic layered materials such as BN, MoS_2, WS_2, $MoSe_2$, $MoTe_2$, $TaSe_2$, $NbSe_2$ and $NiTe_2$.[7] By adopting a modified liquid exfoliation method, Xie et al. successfully synthesized monolayer VS_2[8,9] and SnS_2,[10] as well as monolayer structures of nonlayered ZnSe and ZnS materials.[11]

Silicon and boron are two nearest-neighbors of carbon in the periodic table, and both are believed to possess 2D monolayer structure (e.g., silicene).[12−22] Silicene has attracted increasing attention recently because of the existence of Dirac fermion[14] and its compatibility with silicon-based nanotechnology. A silicon atom has a larger ionic radius than carbon, which tends to promote sp^3 hybridization. As a result, free-standing monolayer silicene prefers a low-buckled structure,[14,15,23] although bilayer hexagonal silicon can be a metastable planar structure when formed within a slit nanopore as suggested from a previous classical molecular dynamics simulation.[24] Although silicene may not be isolated by using the exfoliation method as for the graphene, silicene nanoribbons fabricated by deposition of silicon atoms on a Ag(110) surface have been reported in the literature.[25−28] Very recently, epitaxial growth of silicene sheets on Ag(111)[29−31] and NbB_2(0001)[32] substrate has also been realized in the laboratory. It was found that the silicene sheet on Ag(111) surface has similar electronic properties as the graphene, such as the electronic dispersion resemblance to relativistic Dirac fermions,[31] and that on NbB_2(0001) surface, a direct π-electronic band gap is detected.[32] Recently, many low-energy forms of 2D monolayer boron have been predicted,[16−21] namely, α-sheet, $g_{1/8}$ and $g_{2/15}$ sheets, and α_1-, α_2-, β_1-, and β_2-sheets, whose cohesive energies are nearly degenerate with each other (though predicted relativities are functional dependent). These 2D boron sheets can be viewed as selective removal of boron atoms from a closed-packed triangular boron sheet. Most of these monolayer sheets are predicted to be flat and metallic, except for the α-sheet, which is a nonplanar buckled structure with a modest band gap (semiconducting).[21] Besides elemental boron and silicon, monolayer structures of boron−carbon

Received: December 4, 2012
Accepted: January 28, 2013
Published: January 31, 2013

   dx.doi.org/10.1021/jz302000q | J. Phys. Chem. Lett. 2013, 4, 561−567

compounds,[33,34] Si_2C,[35] nitrogen-graphene alloys,[36] ZnO,[37] and group III−V compounds[38,39] have also been predicted.

Because boron is one of the most important p-type dopants used in silicon industry, boron−silicon compounds have attracted considerable attention. The existence of silicon−boron compounds was reported more than a century ago. Moissan and Stock discovered SiB_3 and SiB_6 through fusion of the elements.[41] A more well-known silicon boride is SiB_4, which was first reported in 1960.[42] The crystalline structures of silicon borides are closely related to the boron icosahedra structure. For example, SiB_3 is based on 12-atom, boron rich icosahedra in which some boron atoms are substituted by silicon atoms. SiB_4 is isomorphic to B_4C, and it is composed of Si−B−Si chains and B_{12} icosahedra. Additionally, the crystal structure of SiB_6 contains icosahedra, icosihexahedra, as well as isolated silicon and boron atoms. These B−Si compounds are also known for their mechanical hardness. More recently, theoretical calculations have been performed to investigate properties of boron-doped silicon nanocrystal[42] and cubic silicon.[43]

Since both boron and silicon can possess 2D monolayer structure, boron-doped silicene or silicon-doped boron sheets are likely to exist. Very recently, Hansson et al. reported a 2D BN-like hexagonal SiB crystal (*h*-SiB).[44] To determine whether this structure is the ground-state or not requires a global search of all the low-energy structures of 2D BSi. Another question is whether the boron−silicon compounds can possess a planar monolayer structure at certain stoichiometry. To address this question, we adopt a global optimization method based on the particle-swarm optimization (PSO) techniques[45] to predict 2D structures of silicon−boron compounds with a wide distribution of B composition. The lowest-energy monolayer structures of BSi_4, BSi_3, BSi_2, BSi, B_2Si, B_3Si, B_4Si, B_5Si, B_6Si, and B_7Si are predicted, and the B−Si compounds with higher boron composition are energetically more preferable due to higher cohesive energies. Moreover, our density functional theory (DFT) calculations suggest that all these monolayer boron−silicon compounds are metallic. Interestingly, in the predicted monolayer structures of BSi_4, BSi_3, BSi, BSi_2, BSi_3, BSi_5 and BSi_6, each Si atom is bonded with three B or Si atoms within the same plane, representing a preference of the planar sp^2-bonding for Si in 2D B−Si compounds. On the other hand, BSi_2 and B_4Si monolayers exhibit a small out-of-plane buckling.

Geometrical Properties. 2D B−Si compounds with 10 different B−Si stoichiometric compositions are considered, namely, BSi_4, BSi_3, BSi_2, BSi, B_2Si, B_3Si, B_4Si, B_5Si, B_6Si, and B_7Si. The predicted lowest-energy structures are shown in Figure 1, and other low-energy structures (for BSi_3 and B_3Si, only one stable structure is found) are illustrated in the Supporting Information (Figures S1−S8). Here, we use I, II, and III to label the energy ranking of the low-energy structures (for example, BSi_4-I denotes the lowest-energy structure, and BSi_4-II is the second low-lying structure). Note that the lowest-energy structure possesses the greatest cohesive energy.

For silicon-rich compounds, i.e., BSi_4, BSi_3 and BSi_2, their structures can be viewed as boron-doped graphene-like silicon monolayers. The lowest-energy BSi_4 (BSi_4-I) exhibits a planar graphene-like structure that is composed of parallel armchair-type silicon nanoribbons separated by boron-dimer chains, as shown in Figure 1a. Although the free-standing silicene is known to exhibit a weakly buckled structure, it is interesting that the silicon nanoribbons in BSi_4-I can be stabilized within the same plane through connecting with boron dimer chains. Here we do not use the term silicene ribbon because it may give a false impression that the nanorribons assume the nonplanar buckled structure.

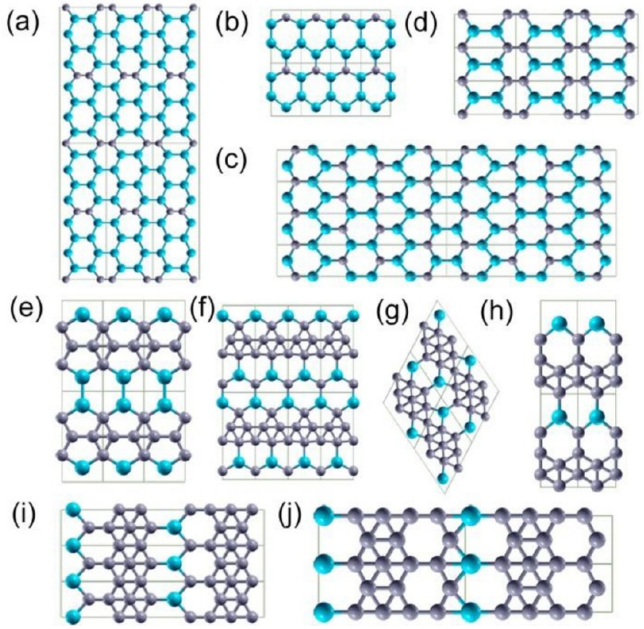

Figure 1. Predicted lowest-energy monolayer structures of (a) BSi_4-I, (b) BSi_3-I, (c) BSi_2-I, (d) BSi-I, (e) B_2Si-I, (f) B_3Si-I, (g) B_4Si-I, (h) B_5Si-I, (i) B_6Si-I, and (j) B_7Si-I from the PSO structural search. Si and B atoms are denoted by cyan and gray spheres.

In BSi_4-II structure, silicon atoms form square rings, and each boron atom is bonded with four silicon square rings at their corner, i.e., silicon and boron atoms are packed into a mosaic of square silicon rings and hexagonal B_2Si_4 rings (see Figure S1). Different from BSi_4-I, the structure of BSi_4-II is weakly buckled with an out-of-plane distance of 0.75 Å. The BSi_4-III monolayer is strictly planar, and the silicon and boron atoms are packed into a mosaic of silicon rhombus rings and hexagonal B_2Si_4 rings with two neighboring rhombus rings sharing a planar-tetracoordinated silicon (ptSi) atom, akin to the planar-tetracoordinated carbon (ptC).[46] Hence, 25% silicon atoms are bonded with four silicon atoms, forming the planar-tetracoordinated structure similar to that of the previously reported 2D boron-carbide sheet and SiC_2 sheet.[33−35] Note that the existence of ptSi atoms with Si−Si bonds has not been reported in the literature. Our DFT calculation indicates that BSi_4−I is energetically more favorable than BSi_4-II and BSi_4-III by 95.0 meV/atom and 103.2 meV/atom, respectively. The large differences in the cohesive energy might be due to the presence of the silicon squares and rhombus in BSi_4-II and BSi_4-III, respectively.

For BSi_3 (Figure 1b), only one stable monolayer structure is obtained based on the PSO global search. This planar structure can be viewed as an alternate arrangement of zigzag single-Si-atom chains and silicon−boron chains. In BSi_2-I and BSi_2-II (Figure 1c and Figure S2), the zigzag single-Si-atom chains are separated by B−Si nanoribbon-composed B_3Si_3 six-membered rings. However, the BSi_2-I is slightly buckled with an out-of-plane distance of about 0.29 Å. The structural difference between BSi_2-I and BSi_2-II is the atomic arrangement of boron and silicon in the six-membered rings. BSi_2-I is energetically more stable than BSi_2-II by 21.1 meV/atom.

When the mole fraction of boron and silicon is the same (BSi), the compound has two competing monolayer structures.

dx.doi.org/10.1021/jz302000q | *J. Phys. Chem. Lett.* 2013, 4, 561−567

The 2D *h*-SiB[44] predicted by Hanson et al. is identical to BSi-II, which possesses a slightly smaller cohesive energy (about 5 meV/atom) than that of BSi-I. Both BSi-I and BSi-II exhibit strictly planar honeycomb structure like graphene. The structure of BSi-I (Figure 1d) is composed of uniformly distributed boron-dimer and silicon-dimer, while in BSi-II, the boron and silicon atoms are distributed alternately in the honeycomb lattice (Figure S3). Their relative stability suggests that in the BSi sheet, B−B and Si−Si bonds are energetically favorable. Since only BSi-I has Si−Si and B−B bonding, it will result in a distinct vibration signal that may be used to differentiate itself from other B−Si compounds once synthesized.

For B-rich systems, boron atoms present multibonding structural characteristics and form ribbon or cluster structures. For B_2Si, the structure of B_2Si-I has an alternate arrangement of one-dimensional (1D) linear boron-atom chains and B_2Si_4 hexagonal-ring chains. Moreover, the neighboring four boron atoms form B_4 rhombus, as shown in Figure 1(e). The B_2Si-II has a similar structure as that of B_2C, but with different arrangement of silicon and boron atoms.[33] For B_2Si-III, the structure is similar to that of B_2Si−I, which has an alternate arrangement of B_3Si_3 hexagonal-ring chains and atomic boron chains (see Figure S4). B_2Si-I is energetically more favorable than B_2Si-II and B_2Si-III by 59.8 meV/atom and 75.1 meV/atom, respectively. The existence of Si−Si π bonding in B_2Si-I (with a Si−Si bond length of 2.30 Å) may help stabilization of the structure. In B_2Si-III, silicon exhibits two bonding characteristics, a planar sp^2 bonding and an inequivalent planar-tetracoordinated bonding.

For B_3Si, only one stable monolayer structure is found from the PSO global search. The structure of B_3Si sheet has an alternate arrangement of narrow boron ribbons and B_3Si_3 hexagonal-ring chains (Figure 1f). The planar structure contains B_3Si_3 six-membered rings, B_4Si five-membered rings, B_4Si_2 six-membered rings, and boron triangles. The Si atoms are isolated in the structure, and thus only B−Si and B−B bonds exist in the sheet.

From B_4Si to B_7Si, their monolayer sheets have one common structural feature, that is, all structures can be viewed as parallel boron ribbons connected by silicon atoms or silicon−boron dimers (Figure 1g−j, and Figures S5−S8). In B_4Si-I (Figure 1g), boron atoms form 1D prismatic B_9 chains and the parallel B_9 chains are covalently connected via sparse Si−B bonds. The structure of B_4Si-III is composed of two zigzag double-B-atomic chains and one single-Si-atomic chain in the unit cell. An exception is the metastable B_4Si-II, which contains B_3Si_2 five membered rings, B_5Si six-membered rings, B_6Si seven-membered rings, and boron triangles. The B_3Si_2 rings in the sheet form 1D infinite chain. B_4Si-I is energetically more favorable than B_4Si-II and B_4Si-III by 16.8 and 24 meV/atom, respectively. Additionally, B_4Si-I is slightly buckled (the largest out-of-plane distance is 0.54 Å), while B_4Si-II and B_4Si-III are dynamically stable in the planar form.

The energy difference between the two predicted low-energy structures of B_5Si is less than 1 meV/atom, indicating polymorphic nature of B_5Si sheet. The structure of B_5Si-I has an alternate arrangement of zigzag BSi atomic chain and double-B-atomic chains (Figure 1h). B_5Si-II has a similar structure as B_2Si−II with less silicon composition, which is composed of 1D prismatic B_4 and B_3Si chains (Figure S6). Si atoms in B_5Si-II sheet are planar tetracoordinated.

For B_6Si, the lowest-energy structure (B_6Si-I) can be viewed as a stacking of BSi zigzag chains and edge-sharing B_7 hexagon (B_6 hexagon with an extra B at center) chains. Connected with edge boron atoms in the B_7 chain, B and Si atoms in the BSi chain form B_5Si and B_4Si_2 (with Si at 1, 3 positions) six-membered rings. Metastable B_6Si-II has a similar structure as B_4Si-I, which contains B_6Si seven-membered rings and B_4Si five-membered rings. The structure of B_6Si-III can be viewed as zigzag prismatic B_4 chains connected by Si atoms with large B_6Si_2 holes. B_6Si-II and B_6Si-III have a higher energy of 34 meV/atom and 39.4 meV/atom, respectively, than B_6Si-I. The structure of B_7Si is closely related to that of B_5Si. If one inserts 1D zigzag boron chains into the interfacial regions between the building units of B_5Si, B_5Si-I and B_5Si-II would turn into B_7Si-II and B_7Si-I, respectively.

In summary, 2D boron−silicon sheets present versatile morphologies depending on the Si−B stoichiometry. (1) For Si-rich and B−Si compounds, a general structural feature of 2D sheets is a graphene-like honeycomb with various arrangements of boron and silicon atoms. B−B and Si−Si bonding are energetically favored. (2) For B-rich compounds, boron atoms prefer to form ribbon structures due to the tendency of multibonding characteristic of boron while silicon atoms prefer to form single-atomic chain by itself (single-Si-atomic chain) or with boron (BSi atomic chain). (3) Silicon can form planar-tetracoordinated bonding structure with boron or other silicon atoms. Especially, ptSi surrounded by four silicon atoms is predicted to be stable in the metastable BSi_4-III sheet and B_5Si-II sheet, as well as B_7Si-I sheet. (4) Except for BSi_2, B_4Si, and B_7Si, silicon atoms in the lowest-energy B−Si sheets favor sp^2 hybridization.

Structural Stability. To confirm the structural stability of predicted 2D boron silicon sheets, we perform lattice dynamics calculations (phonon-spectrum calculations at 0 K) using the linear response theory.[47] Note that at low temperature, all vibrational motions in the crystal can be decomposed into nearly independent phonon modes (i.e., normal modes). Therefore, at low temperature, phonon instability is both necessary and sufficient conditions for mechanical instability of a crystal. No imaginary phonon frequencies are observed in the Brillouin zone for all 2D B−Si compounds (see Figure 2 for representative phonon band structures), indicating the inherent dynamical stability of these B−Si sheets. The highest zone-center phonon frequencies are 792 cm^{-1}, 1036 cm^{-1}, and 1234 cm^{-1} for BSi_2-I, BSi-I, and B_2Si-I, respectively. The lower frequency for BSi_2-I than that of BSi-I and B_2Si-I is due to the difference in bonding type. For BSi-I and B_2Si-I, the phonon mode with the highest frequency is the B−B stretching mode, while for BSi_2-I, it is a B−Si stretching mode. The B−B mode possesses higher frequency due to lighter atomic mass of boron and shorter bond length. The difference in zone-center phonon modes for different 2D B−Si compounds can be used to identify the structures of the compound once synthesized. For example, the highest zone-center phonon mode of BSi-I and B_2Si-I are Raman active modes, while the one for BSi_2 is both Raman and IR active. Hence, some of these phonon modes can be used as a fingerprint in the spectrum to determine structures of 2D B−Si compounds.

To evaluate relative stabilities among the predicted 2D B−Si compounds, we compute their cohesive energies (E_{coh}). Computed values of E_{coh} with respect to boron composition are presented in Figure 3 (see Supporting Information Table S1 for the average cohesive energies of all low-energy boron−

dx.doi.org/10.1021/jz302000q | J. Phys. Chem. Lett. 2013, 4, 561−567

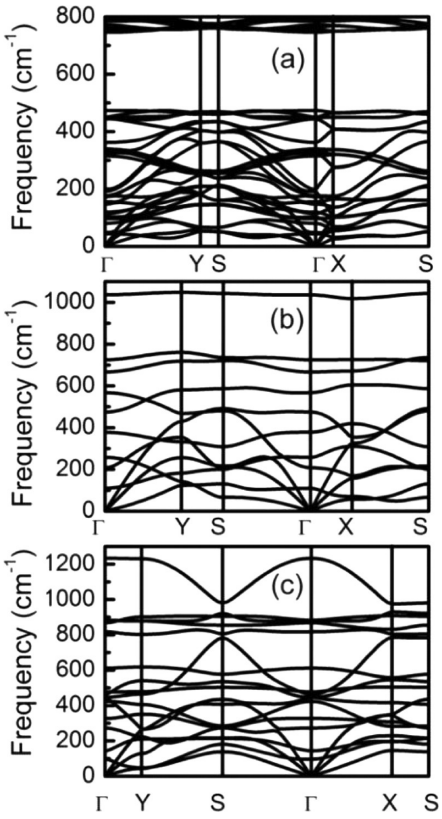

Figure 2. Phonon band structures of (a) BSi_2-I, (b) BSi-I, and (c) B_2Si-I. Γ(0.0, 0.0, 0.0), Y(0, 0.5, 0.0), S(0.5, 0.5, 0), and X(0.5, 0.0, 0.0) refer to special points in the first Brillouin zone.

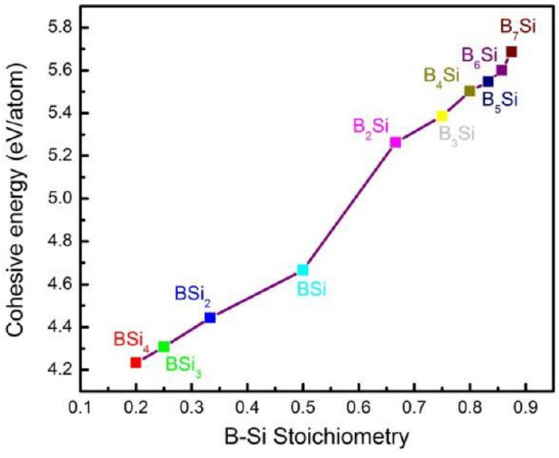

Figure 3. Cohesive energies of the lowest-energy 2D B−Si compounds with respect to B_xSi_y stoichiometry $x/(x+y)$.

silicon sheets). It can be seen that E_{coh} values increase with increasing boron composition. B_7Si has the highest E_{coh} value, suggesting higher structural stability, compared to other B−Si sheets.

Electronic Properties. Electronic band structure calculations suggest that all the 2D B−Si compounds predicted are metallic, as are most 2D boron sheets[16,20,21] and 2D B−C compounds.[33,34] The metallicity stems from the delocalized p_z π electrons of boron and silicon. To gain more insight into the electronic structures, the partial density of states (PDOS) of the 2D B−Si compounds are also analyzed. Representative PDOSs for BSi_2-I, BSi-I, and B_2Si-I are shown in Figure 4. The s and p

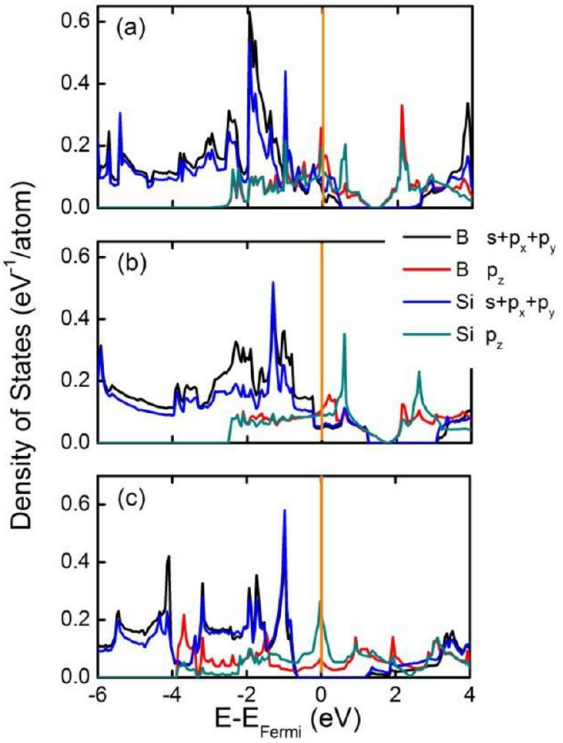

Figure 4. PDOS for (a) BSi_2-I, (b) BSi-I, and (c) B_2Si-I. The vertical orange lines denote the Fermi level.

orbitals are separated into in-plane σ states (the sum of s, p_x, and p_y) and out-of-plane π states (p_z). The mixing between σ and π states is prohibited by the symmetry since, in 2D systems, s, p_x, and p_y orbitals are symmetric with respect to the mirror plane, while p_z is antisymmetric. Clearly, the p_z states in Figure 4 are partially occupied. Another feature in Figure 4 is that the bonding σ states and antibonding σ^* states are well separated. As an example, in BSi_2-I (Figure 4a), the hybrid B−Si bonding σ states end at 0.5 eV (black & blue lines) above the Fermi level, which means the bonding σ states are hole doped, while the antibonding σ^* states start at 2.1 eV (black & blue lines). Similar to BSi_2-I, the hybrid B−Si σ states that end at 1.3 eV above the Fermi level are also hole doped, while the antibonding σ^* states start at 3.1 eV. Interestingly, in B_2Si-I, the bonding σ states are fully occupied, and the antibonding σ^* states are empty. Such a hallmark that the Fermi level lies in the gap of in-plane PDOS has been used previously to explain the stability of the lowest-energy boron sheets since the in-plane bonds formed from overlapping of sp^2 hybrids are stronger than the out-of-plane π bonds.[16,20,21] Here, except for B_2Si-I, we find that the lowest-energy structures of BSi_4 and B_3Si (see Figures S9 and S10) also entail this hallmark electronic feature, i.e., having optimal occupation of in-plane σ states.

To understand the bonding nature of the predicted 2D B−Si compounds, we also perform electron localization function (ELF) analysis.[48,49] We plot iso-surfaces of ELFs for the lowest-energy 2D B−Si compounds with a relatively large iso-value of 0.75 in Figure 5 to highlight the in-plane σ states. For silicon-rich compounds (BSi_4-I, BSi_3-I, and BSi_2-I) and BSi-I, all B and Si atoms are 3-fold coordinated, and the ELF localizes at the bond center of B−Si, Si−Si, and B−B bonds (see Figure 5a−d), similar to the ELF pattern in graphene. For B_2Si-I, we can see clearly one Si−Si σ bond, one B−B two-center σ bond, four B−Si σ bonds, and two three-center B bonds per unit cell. Similar

dx.doi.org/10.1021/jz302000q | J. Phys. Chem. Lett. 2013, 4, 561−567

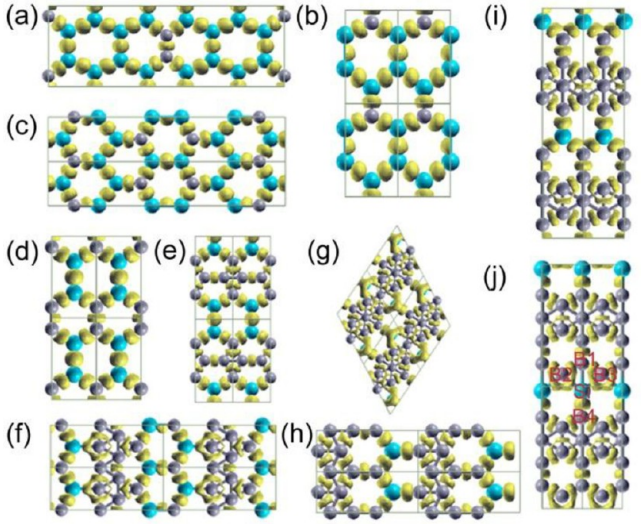

Figure 5. Iso-surfaces of ELF with the value of 0.75 for (a) BSi_4-I, (b) BSi_3-I, (c) BSi_2-I, (d) BSi-I, (e) B_2Si-I, (f) B_3Si-I, (g) B_4Si-I, (h) B_5Si-I, (i) B_6Si-I, and (j) B_7Si-I.

to B_2Si-I, one can see that ELF distributes around the center of boron triangles for boron-rich B_3Si-I, B_5Si-I and B_6Si-I, indicating the existence of boron three center bonds. For B_7Si-I, the ELF around ptSi is mainly distributed over silicon and B_2, B_3, and B_4 (Figure 5j and Figure S12), while the bonding between Si and B_1 appears to be very weak (see ELF and computed deformation electron density in Figure S12c), suggesting a partial fourth bond. Interestingly, although the structures of BSi_2-I and B_4Si-I are buckled, the ELF around silicon atoms shows different characteristics: In BSi_2-I, the ELF localizes at the center of B−Si and Si−Si bonds, while in B_4Si-I, the ELF around the silicon shows a pyramid-like structure, indicating sp^3-like bonding. The sp^3-like bonding of silicon in B_4Si-I is also proven in PDOS of B_4Si-I (see Figure S11), in which the peaks of silicon p_z states and in-plane states clearly show some overlap around −1 and 1.8 eV.

In conclusion, we have performed a global search of monolayer structures of B−Si compounds based on the PSO algorithm combined with first-principles calculations. The most stable structures of 2D B−Si compounds are predicted for a wide range of B−Si stoichiometries, many for the first time. Stabilities of these predicted structures are verified via lattice dynamics calculations as well as electronic structure calculations. Our calculations suggest that (1) all 2D B−Si compounds are metallic; (2) the structures of silicon-rich 2D B−Si compounds and BSi are likely to exhibit a graphene-like honeycomb structure, while in boron-rich 2D B−Si compounds, boron atoms tend to form triangles as in 2D boron sheets; (3) except for BSi_2, B_4Si, and B_7Si, silicon atoms in 2D B−Si compounds favor sp^2 hybridization. To our knowledge, such a preference to sp^2 bonded silicon in low-dimensional condensed matter has not been previously reported in the literature. If confirmed, this prediction will enrich the family of silicon chemical structures, in light of the fact that silicon tends to form multiple bonds and hyper-coordinated bonds.

■ COMPUTATIONAL METHODS

PSO Calculations. The PSO algorithm within the evolutionary scheme as implemented in the CALYPSO (Crystal structure AnaLYsis by Particle Swarm Optimization) code[45] is employed to search for low-energy structures of 2D boron−silicon compounds. As an unbiased global optimization method, the PSO algorithm was inspired by the choreography of a bird flock and can be viewed as a distributed-behavior algorithm that performs multidimensional search.[50] We selected the PSO algorithm because it is very fast and efficient compared to other methods, and it requires few parameters to adjust.[51] The PSO algorithm, coupled with DFT optimization, has been utilized in predicting low-energy structures of 2D boron-carbide compounds,[34] 2D boron sheets,[21] as well as 3D structures of elements and compounds.[52−54] In the PSO structural search, the population size is set to be 30, and the number of generation is maintained at 30. All possible supercell sizes are considered with the total number of atoms no more than 20 in the supercell. As an example, for BSi, supercells with up to 10 unit-cells are considered. In the first generation, random structures are constructed by generating atomic coordinates using crystallographic symmetry operations. Next, the structures are optimized using a DFT method (below). Third, the best 60% structures are selected by PSO to generate the next generation, and other structures in the new generation are generated randomly, which guarantee the structural diversity.

DFT Calculations. DFT within PBE-type general gradient approximation (GGA) as implemented in VASP 5.2[55,56] is used to relax the structures and compute the cohesive energies. The ion-electron interaction is treated using the projector augment wave (PAW) technique. For geometric optimization, both lattice constants and atomic positions are relaxed until the forces on atoms are less than 0.02 eV /Å and the total energy change is less than 1.0×10^{-5} eV. The vacuum distance is set to about 20 Å to neglect the interlayer interaction. The Brillouin zone is sampled using k-points with 0.02 $Å^{-1}$ spacing in the Monkhorst−Pack scheme.[57] For the cohesive energy calculation, we used the formula $E_{coh} = (xE_B + yE_{Si} - E_{B_xSi_y})/(x + y)$, where E_B, E_{Si}, and E_{BxSiy} are total energies of a single B-atom, a single Si-atom, and 2D B_xSi_y compound (per unit cell), respectively. Previous benchmarks on eight simple main-group solids show that PBE-type GGA underestimates the cohesive energies by −0.04 eV/atom on average, which is almost exact.[58] ELF analysis is used to understand the bonding nature of 2D B−Si compounds. Note that ELF is related to the total electron density and its gradient. The topological analysis of ELFs has been shown to be a rigorous approach to distinguishing different chemical bonds. ELF values range from 0 to 1 according to the definition, and for localized in-plane σ states, the ELF value should be close to 1, while for delocalized π state, the ELF value should be smaller than 0.5.

Phonon Spectrum Calculations. In the PSO structure search, each system is constrained to a plane. This constraint is removed during the geometrical optimization in DFT calculations. So it is still conceivable that the predicted structures are not a local minimum due to the removal of the constraint and prefer out-of-plane buckling. To ensure predicted structures are local minima, we carry out phonon spectrum calculations to examine the dynamical stability of all predicted low-energy structures. The phonon spectra are computed based a DFT perturbation method with the linear response as implemented in the QUANTUM ESPRESSO package.[47] We collect the structures without imaginary phonon modes, and for the structures having imaginary modes at the Γ point, we distort positions of the atoms along the vibration

dx.doi.org/10.1021/jz302000q | J. Phys. Chem. Lett. 2013, 4, 561−567

eigenvectors of the zone center soft phonon mode to achieve a new stable structure.

■ ASSOCIATED CONTENT

Supporting Information

Table of calculated cohesive energies, low-energy structures of 2D B−Si compounds, ELF for BSi_2-I and B_7Si-I, and PDOS for BSi_4-I, B_3Si-I, and B_4Si-I are collected. This material is available free of charge via the Internet at http://pubs.acs.org.

■ AUTHOR INFORMATION

Corresponding Author

*E-mail: xjwu@ustc.edu.cn (X.W.); zeng1@unl.edu (X.C.Z.).

Notes

The authors declare no competing financial interest.

■ ACKNOWLEDGMENTS

USTC group is supported by the National Basic Research Programs of China (Nos. 2011CB921400, 2012CB 922001), the NSFC (Grant Nos. 21121003, 11004180, 51172223), the One Hundred Person Project of CAS, the Shanghai Supercomputer Center, and the Hefei Supercomputer Center. The UNL group is supported by ARL (Grant No. W911NF1020099), NSF (Grant No. DMR-0820521), and a grant from USTC for (1000plan) Qianren-B summer research.

■ REFERENCES

(1) Novoselov, K. S.; Geim, A. K.; Morozov, S. V.; Jiang, D.; Zhang, Y.; Dubonos, S. V.; Grigorieva, I. V.; Firsov, A. A. Electric Field Effect in Atomically Thin Carbon Films. *Science* **2004**, *306*, 666−669.

(2) Novoselov, K. S.; Geim, A. K.; Morozov, S. V.; Jiang, D.; Katsnelson, M. I.; Grigorieva, I. V.; Dubonos, S. V.; Firsov, A. A. Two-Dimensional Gas of Massless Dirac Fermions in Graphene. *Nature* **2005**, *438*, 197−200.

(3) Novoselov, K. S.; McCann, E.; Morozov, S. V.; Falko, V. I.; Katsnelson, M. I.; Zeitler, U.; Jiang, D.; Schedin, F.; Geim, A. K. Unconventional Quantum Hall Effect and Berry's Phase of 2π in Bilayer Graphene. *Nat. Phys.* **2006**, *2*, 177−180.

(4) Zhang, Y. B.; Tan, Y. W.; Stormer, H. L.; Kim, P. Experimental Observation of the Quantum Hall Effect and Berry's Phase in Graphene. *Nature* **2005**, *438*, 201−204.

(5) Jin, C.; Lin, F.; Suenaga, K.; Iijima, S. Fabrication of a Freestanding Boron Nitride Single Layer and Its Defect Assignments. *Phys. Rev. Lett.* **2009**, *102*, 195505.

(6) Mak, K. F.; Lee, C.; Hone, J.; Shan, J.; Heinz, T. F. Atomically Thin MoS_2: A New Direct-Gap Semiconductor. *Phys. Rev. Lett.* **2010**, *105*, 136805.

(7) Coleman, J. N.; Lotya, M.; O'Neill, A.; Bergin, S. D.; King, P. J.; Khan, U.; Young, K.; Gaucher, A.; De, S.; Smith, R. J.; et al. Two-Dimensional Nanosheets Produced by Liquid Exfoliation of Layered Materials. *Science* **2011**, *331*, 568−571.

(8) Feng, J.; Sun, X.; Wu, C.; Peng, L.; Lin, C.; Hu, S.; Yang, J.; Xie, Y. Metallic Few-Layered VS_2 ultrathin Nanosheets: High Two-Dimensional Conductivity for In-plane Supercapacitors. *J. Am. Chem. Soc.* **2011**, *133*, 17832−17838.

(9) Feng, J.; Peng, L.; Wu, C.; Sun, X.; Hu, S.; Lin, C.; Dai, J.; Yang, J.; Xie, Y. Giant Moisture Responsiveness of VS_2 Ultrathin Nanosheets for Novel Touchless Positioning Interface. *Adv. Mater.* **2012**, *24*, 1969−1974.

(10) Sun, Y.; Cheng, H.; Gao, S.; Sun, Z.; Liu, Q.; Liu, Q.; Lei, F.; Yao, T.; He, J.; Wei, S.; et al. Freestanding Tin Disulfide Single-Layers Realizing Efficient Visible-Light Water Splitting. *Angew. Chem., Int. Ed.* **2012**, *51*, 8727−8731.

(11) Sun, Y.; Sun, Z.; Gao, S.; Cheng, H.; Liu, Q.; Piao, J.; Yao, T.; Wu, C.; Hu, S.; Wei, S.; et al. Fabrication of Flexible and Freestanding Zinc Chalcogenide Single Layers. *Nat. Commun.* **2012**, *3*, 1057.

(12) Takeda, K.; Shiraishi, K. Theoretical Possibility of Stage Corrugation in Si and Ge Analogs of Graphite. *Phys. Rev. B* **1994**, *50*, 14916.

(13) Guzmán-Verri, G. G.; Lew Yan Voon, L. C. Electronic Structure of Silicon-Based Nanostructures. *Phys. Rev. B* **2007**, *76*, 075131.

(14) Cahangirov, S.; Topsakal, M.; Akturk, E.; Sahin, H.; Ciraci, S. Two- and One-Dimensional Honeycomb Structures of Silicon and Germanium. *Phys. Rev. Lett.* **2009**, *102*, 236804.

(15) Sahin, H.; Cahangirov, S.; Topsakal, M.; Bekaroglu, E.; Akturk, E.; Senger, R. T.; Ciraci, S. Monolayer Honeycomb Structures of Group-IV Elements and III-V Binary Compounds: First-Principles Calculations. *Phys. Rev. B* **2009**, *80*, 155453.

(16) Tang, H.; Ismail-Beigi, S. Novel Precursors for Boron Nanotubes: The Competition of Two-Center and Three-Center Bonding in Boron Sheets. *Phys. Rev. Lett.* **2007**, *99*, 115501/1−4.

(17) Tang, H.; Ismail-Beigi, S. First-Principles Study of Boron Sheets and Nanotubes. *Phys. Rev. B* **2010**, *82*, 115412.

(18) Miller, J. New Sheet Structures May be the Basis for Boron Nanotubes. *Phys. Today* **2007**, *60*, 20−21.

(19) Özdoğan, C.; Mukhopadhyay, S.; Hayami, W.; Güvenç, Z. B.; Pandey, R.; Boustani, I. The Unusually Stable B_{100} Fullerene, Structural Transitions in Boron Nanostructures, and a Comparative Study of α- and γ-Boron and Sheets. *J. Phys. Chem. C* **2010**, *114*, 4362−4375.

(20) Penev, E. S.; Bhowmick, S.; Sadrzadeh, A.; Yakobson, A. I. Polymorphism of the Two-Dimensional Boron. *Nano Lett.* **2012**, *12*, 2441.

(21) Wu, X.; Dai, J.; Zhao, Y.; Zhuo, Z.; Yang, J.; Zeng, X. Two-Dimensional Boron Monolayer Sheets. *ACS Nano* **2012**, *6*, 7443−7453.

(22) Zhang, P.; Li, X. D.; Hu, C. H.; Wu, S. Q.; Zhu, Z. Z. First-Principles Studies of the Hydrogenation Effects in Silicene Sheets. *Phys. Lett. A* **2012**, *376*, 1230−1233.

(23) Lalmi, B.; Oughaddou, H.; Enriquez, H.; Kara, A.; Vizzini, S.; Ealet, B.; Aufray, B. Epitaxial Growth of a Silicene Sheet. *Appl. Phys. Lett.* **2010**, *97*, 223109.

(24) Bai, J.; Tanaka, H.; Zeng, X. C. Graphene-like Bilayer Hexagonal Silicon Polymorph. *Nano Res.* **2010**, *3*, 694−700.

(25) De Padova, P.; Quaresima, C.; Perfetti, P.; Olivieri, B.; Leandri, C.; Aufray, B.; Vizzini, S.; Le Lay, G. Growth of Straight, Atomically Perfect, Highly Metallic Silicon Nanowires with Chiral Asymmetry. *Nano Lett.* **2008**, *8*, 271−275.

(26) Aufray, B.; Kara, A.; VIzzini, S.; Oughaddou, H.; Léandri, C.; Ealet, B.; Le Lay, G. Graphene-like Silicon Nanoribbons on Ag(110): A Possible Formation of Silicene. *Appl. Phys. Lett.* **2010**, *96*, 183102.

(27) De Padova, P.; Quaresima, C.; Ottaviani, C.; Sheverdyaeva, P. M.; Moras, P.; Carbone, C.; Topwal, D.; Olivieri, B.; Kara, A.; Oughaddou, H.; et al. Evidence of Graphene-like Electronic Signature in Silicene Nanoribbons. *Appl. Phys. Lett.* **2010**, *96*, 261905.

(28) De Padova, P.; Quaresima, C.; Olivieri, B.; Perfetti, P.; Le Lay, G. sp^2-like Hybridization of Silicon Valence Orbitals in Silicene Nanoribbons. *Appl. Phys. Lett.* **2010**, *98*, 081909.

(29) Vogt, P.; De Padova, P.; Quaresima, C.; Avila, J.; Frantzeskakis, E.; Asensio, M. C.; Resta, A.; Ealet, B.; Le Lay, G. Silicene: Compelling Experimental Evidence for Graphenelike Two-Dimensional Silicon. *Phys. Rev. Lett.* **2012**, *108*, 155501.

(30) Feng, B.; Ding, Z.; Meng, S.; Yao, Y.; He, X.; Cheng, P.; Chen, L.; Wu, K. Evidence of Silicene in Honeycomb Structures of Silicon on Ag(111). *Nano Lett.* **2012**, *12*, 3507−3511.

(31) Chen, L.; Liu, C. C.; Feng, B.; He, X.; Cheng, P.; Ding, Z.; Meng, S.; Yao, Y.; Wu, K. Evidence for Dirac Fermions in a Honeycomb Lattice Based on Silicon. *Phys. Rev. Lett.* **2012**, *109*, 056804.

(32) Fleurence, A.; Friedlein, R.; Ozaki, T.; Kawai, H.; Wang, Y.; Kamada-Takamura, Y. Experimental Evidence for Epitaxial Silicene on Diboride Thin Films. *Phys. Rev. Lett.* **2012**, *108*, 245501.

(33) Wu, X.; Pei, Y.; Zeng, X. C. B_2C Graphene, Nanotubes and Nanoribbons. *Nano Lett.* **2009**, *9*, 1577−1582.

(34) Luo, X.; Yang, J.; Liu, H.; Wu, X.; Wang, Y.; Ma, Y.; Wei, S. H.; Gong, X.; Xiang, H. Predicting Two-Dimensional Boron−Carbon Compounds by Global Optimization Method. *J. Am. Chem. Soc.* **2011**, *133*, 16285−16290.
(35) Li, Y.; Li, F.; Zhou, Z.; Chen., Z. SiC_2 Silagraphene and Its One-Dimensional Derivatives: Where Planer Tetracoordinate Silicon Happens. *J. Am. Chem. Soc.* **2011**, *133*, 900−908.
(36) Xiang, H.; Huang, B.; Li, Z. Y.; Wei, S. H.; Yang, J. L.; Gong, X. G. Ordered Semiconducting Nitrogen−Graphene Alloys. *Phys. Rev. X* **2012**, *2*, 011003.
(37) Topsakal, M.; Cahangirov, S.; Bekaroglu, E.; Ciraci, S. First-Principles Study of Zinc Oxide Honeycomb Structures. *Phys. Rev. B* **2009**, *80*, 235119.
(38) Li, H.; Dai, J.; Li, J.; Zhang, S.; Zhou, J.; Zhang, L.; Chu, W.; Chen, D.; Zhao, H.; Yang, J.; et al. Electronic Structures and Magnetic Properties of GaN Sheets and Nanoribbons. *J. Phys. Chem. C* **2010**, *114*, 11390−11394.
(39) Şahin, H.; Cahangirov, S.; Topsakal, M.; Bekaroglu, E.; Akturk, E.; Senger, R. T.; Ciraci, S. Monolyer Honeycomb Structures of Group-IV Elements and III−V Binary Compounds: First-Principles Calculations. *Phys. Rev. B* **2009**, *80*, 155453.
(40) Moissan, H.; Stock, A. Preparation and Properties of Two Silicon Borides: SiB_3 and SiB_6. *C. R. Acad. Sci., Paris* **1900**, *131*, 139.
(41) Cline, C. F.; Sands, D. E. New Silicon Boride, SiB_4. *Nature* **1960**, *185*, 456.
(42) Pi, X.; Chen, X.; Yang, D. First-Principles Study of 2.2 nm Silicon Nanocrystals Doped with Boron. *J. Phys. Chem. C* **2011**, *115*, 9838−9843.
(43) Bourgeois, E.; Blasé, X. Superconductivity in Doped Cubic Silicon: An *Ab Initio* Study. *Appl. Phys. Lett.* **2007**, *90*, 142511.
(44) Hansson, A.; de Brito Mota, F.; Rivelino, R. Metallic Behavior in Low-Dimensional Honeycomb SiB Crystal: A First-Principles Prediction of Atomic Structure and Electronic Properties. *Phys. Rev. B* **2012**, *86*, 195416.
(45) Wang, Y. C.; Lv, J.; Zhu, L.; Ma, Y. M. Crystal Structure Prediction via Particle-Swarm Optimization. *Phys. Rev. B* **2010**, *82*, 094116.
(46) Schleyer, P. v. R.; Boldyrev, A. I. A New General Strategy for Achieving Planar Tetracoordinate Geometries for Carbon and Other Second Row Periodic Elements. *J. Chem. Soc., Chem. Comm.* **1991**, 1536−1538.
(47) Giannozzi, P.; Baroni, S.; Bonini, N.; Calandra, M.; Car, R.; Cavazzoni, C.; Ceresoli, D.; Chiarotti, G. L.; Cococcioni, M.; Dabo, I.; et al. QUANTUM ESPRESSO: A Modular and Open-Source Software Project for Quantum Simulations of Materials. *J. Phys.: Condens. Matter.* **2009**, *21*, 395502/1−19.
(48) Silvi, B.; Savin, A. Classification of Chemical Bonds Based on Topological Analysis of Electron Localization Functions. *Nature* **1994**, *371*, 683.
(49) Savin, A.; Nesper, R.; Wenger, S.; Fässler, T. F. ELF: The Electron Localization Function. *Angew. Chem., Int. Ed.* **1997**, *36*, 1808−1832.
(50) Kennedy, J. Eberhart, R. C. Particle Swarm Optimization. *Proceedings of the IEEE International Conference on Neural Network*, Piscataway, NJ, 1995; pp 1942−1948.
(51) http://www.swarmintelligence.org/
(52) Zhu, L.; Wang, H.; Wang, Y.; Lv, J.; Ma, Y.; Cui, Q.; Ma, Y.; Zou, G. Substitutional Alloy of Bi and Te at High Pressure. *Phys. Rev. Lett.* **2011**, *106*, 145501.
(53) Zhu, L.; Wang, Z.; Wang, Y.; Zou, G.; Mao, H.; Ma, Y. Spiral Chain O_4 Form of Dense Oxygen. *Proc. Natl. Acad. Sci.U.S.A.* **2012**, *109*, 751−753.
(54) Zhou, R. L.; Zeng, X. C. Polymorphic Phase of sp^3-Hybridized Carbon under Cold Compression. *J. Am. Chem. Soc.* **2012**, *134*, 7530−7538.
(55) Kresse, G.; Furthmüller, J. Efficiency of *Ab Initio* Total Energy Calculations for Metals and Semiconductors Using a Plane-Wave Basis Set. *J. Comput. Mater. Sci.* **1996**, *6*, 15−50.
(56) Kresse, G.; Furthmüller, J. Efficient Iterative Schemes for *Ab Initio* Total-Energy Calculations Using a Plane-Wave Basis Set. *Phys. Rev. B* **1996**, *54*, 11169−11186.
(57) Monkhorst, H. J.; Pack, J. D. Special Points for Brillouin-Zone Integrations. *Phys. Rev. B* **1976**, *13*, 5188−5192.
(58) Csonka, G.; Perdew, J.; Ruzsinszky, A.; Philipsen, P.; Lebègue, S.; Paier, J.; Vydrov, O.; Ángyán, J. Accessing the Performance of Recent Density Functionals for Bulk Solids. *Phys. Rev. B* **2009**, *79*, 155107.